Calibration of a 2-D morphodynamic model using water–sediment flux maps derived from an ADCP recording

Massimo Guerrero, Vittorio Di Federico and Alberto Lamberti

ABSTRACT

This study compared numerical simulations of the hydro-morphodynamics of a stretch of the Po River (Italy) to detailed measurements of the river's morphology and water–sediment fluxes. A survey of the 8-km-long, 250-m-wide river section, previously described in former publications, was performed using two vessels. The first was equipped with a multibeam echo sounder for bathymetry and the investigation of bed forms, while the second was equipped with two acoustic Doppler current profilers (ADCPs) to map bed roughness, flow velocity, and suspended sediment fields. This paper focuses on the calibration of the shallow water numerical model MIKE21C implemented by the Danish Hydraulic Institute. Sensitivity analyses were performed to analyze the effects of bed roughness and sediment transport direction on the simulated flow field and morphology. The results fixed the predominant flow and morphology parameters in the model, and show how the velocity and sediment field maps that were derived from the ADCP recording could be used for calibration and validation of the existing software.

Key words | ADCP, morphodynamics calibration, Po River, sediment transport direction

Massimo Guerrero (corresponding author)
Hydraulic Laboratory,
DICAM,
Bologna University,
via Terracini 28,
40131 Bologna,
Italy
E-mail: *massimo.guerrero@unibo.it*

Vittorio Di Federico
Alberto Lamberti
DICAM,
Bologna University,
viale Risorgimento 2, 40136,
Bologna,
Italy

INTRODUCTION

Changes in a river channel's morphology affect hydraulic engineering structures, and fluvial hydrodynamics and channel morphology have been studied extensively for many years (examples include Jansen *et al.* 1979; Yalin & da Silva 2001; Parker 2004; Guerrero & Lamberti 2006; Garcia 2008). Field techniques and numerical or analytical models have been applied, albeit separately from one another, with the goal of investigating water and sediment fluxes and the corresponding morphodynamics of sandy rivers. Innovative field techniques have overcome, to some degree, the limitations of traditional measurement devices employed in river engineering. Consequently, accurate and extensive survey data can be used to evaluate the detailed results of numerical models.

The innovative instrumentation frequently employed in surveys includes the acoustic Doppler current profiler (ADCP) and multibeam echo sounder (MBES). The ADCP is used in several studies to characterize secondary flows and vertically averaged velocity patterns. In particular, Parsons *et al.* (2005) have described investigations of 3-D channel-bed-form morphology and the corresponding velocity field on the Parana River using a MBES and ADCP, respectively. ADCP measurements have also been used to assess shear stress by fitting the logarithmic velocity profiles of several rivers, including the Parana (Szupiany *et al.* 2007). The spatial distribution of depth-averaged water velocity, secondary flow deviation, and shear velocity have been mapped using ADCPs, with simultaneous investigation of bathymetry and bed forms using MBES, in a long section of the sandy Po River in Italy (Guerrero & Lamberti 2011). Sediment transport has also been investigated using ADCP. Rennie & Church (2010) have utilized an ADCP data to map the shear velocity and apparent bed load of the lower Fraser River in British Columbia, while Szupiany *et al.* (2009) have assessed the suspended sand concentration and secondary flow distributions at certain cross-sections of the Parana. Guerrero *et al.* (2011) have used ADCP backscattering to

doi: 10.2166/hydro.2012.126

Downloaded from https://iwaponline.com/jh/article-pdf/15/3/813/387053/813.pdf
by guest

infer the suspended sediment concentration and grain size in the Parana River.

A variety of free-source and commercial codes are available for the numerical simulation of river morphodynamics. In fact, after three decades of research, the science of computation fluid dynamics (CFD) has yielded a number of well-tested algorithms that are applicable not only to fixed but also to movable bed case studies (contributors include Mosselman 1992; Olsen 1999; Viscardi *et al.* 2006). In large rivers, the cross-sectional width-to-depth ratio typically ranges from 10 to 100. In such cases, the shallow water approximation can be applied to extend the computational domain, leading to two-dimensional (2-D) numerical models (i.e., depth-integrated flow model). Several commercial models are available for this purpose. The Delft Hydraulics and Danish Hydraulic Institute (DHI) software packages simulate the 2-D shallow water flow equations and couple them with a sediment transport module to simulate river bed evolution. These numerical tools are designed to simulate river sections measuring tenths of kilometers over a longer period of time (e.g., 10 years) than that commonly employed with a full 3-D CFD. This type of simulation provides insight into the long-term impacts of changed hydrology and hydraulics on river channels, fluvial navigation, bank stability, and reservoir capacities, but with these advantages comes the disadvantage that certain physical processes must be modeled using approximations. Oversimplifications involving the shear process, secondary flow and sediment transport require thorough verification of the results.

The objective of this study was to illustrate how the measurements from ADCPs could be used for the calibration of existing software, such as the 2-D model (MIKE21C) implemented by DHI. To this end, the results of that model were compared with morphology and stream flow maps of the Po River. The availability of historical data and continuous water level and discharge recordings made the Po River an ideal case study for the verification of novel techniques that could be applied in more remote parts of the world where the body of recorded data is lacking.

The survey of the 8-km-long, 250-m-wide river section, presented in full in Guerrero & Lamberti (2011), was carried out using two vessels in May 2007. The first was equipped with a MBES for bathymetry and bed form investigation, while two ADCPs were located on the second vessel to map velocities and suspended sediment fields. The hydraulic calibration was conducted using steady-state conditions by comparing measured and simulated velocity fields. This calibration was verified against a sensitivity analysis of the bed roughness parameter on the resulting water slope. Further sensitivity analysis was performed on the resulting bathymetry, alternate bar formation, and consequent sorting of transported sediments using 2-year morphodynamic simulations ending on the survey date in May 2007. The parameter values in the morphodynamics model were fixed by comparing surveyed and simulated morphologies and suspended sediment distributions. The study concluded with a discussion of the model limitations encountered and each parameter's effectiveness in changing the simulated morphology, and the usefulness of the water–sediment flux maps derived from ADCP recording was identified.

This paper is organized as follows. The next section presents the study site and measurement instruments and techniques, additional details of which can be found in Guerrero & Lamberti (2011) and Guerrero *et al.* (2011, 2012). A detailed description of the applied mathematical model can be found in DHI (2002), Olesen (1987) and in Talmon (1992), while only the fundamental features most relevant to the calibration in this case study are reported in the section Mathematical model. The section after that briefly introduces the numerical simulations performed, with the subsection focusing on historical data, the water–stage relationship, and water level records that were applied to fix the boundary conditions and assess the flow discharge interval that most affected the channel morphology during the simulated period. The next two sections give the results of the model's application. The first of these sections analyzes the bed roughness and secondary flow parameter calibrations performed using steady-state conditions, and the second reports the results of the morphodynamic simulation spanning the 2 years prior to the survey date. A discussion section elucidates the model's sensitivity to its parameters and the limits encountered in simulating the observed morphology and fields of flow velocity and transported sediment in the river. The final section is a set of conclusions emphasizing the usefulness of the water–sediment flux maps derived from ADCP recording for the

Downloaded from https://iwaponline.com/jh/article-pdf/15/3/813/387053/813.pdf
by guest

calibration of numerical models, such as the MIKE21C, for applications in current river engineering practice.

STUDY SITE AND MEASUREMENT TECHNIQUES

The Po River is the longest river in Italy. Its main channel is 650 km long, and its 71,000-km^2 catchment includes most of the Italian Alpine slopes, the Po Plain (Pianura Padana), and the Emilian slopes of the Apennine mountains, amounting to approximately one-quarter of Italy (Figure 1(a)). The average and historical maximum discharges are approximately 1,500 and 12,000 m^3/s, respectively, and the transport of bed sediment has been estimated to have decreased in the last century from 10×10^6 to 5×10^6 m^3/year based on the past rate of delta extension and land subsidence data (Cati 1981). Figure 2 shows the morphodynamic model domain superimposed on historical cartography dating back to the beginning of the 19th century. The course of the river has changed dramatically over the years. The central channel is maintained for navigation purposes, and discharges up to full bank values are forced to pass through a 200- to 300-m-wide channel, whereas the natural waterway was twice as wide on average. In fact, bed degradation has increased the discharge passing through the navigation channel since the 1960s (Lamberti & Schippa 1994) such that the 250-m-wide navigation channel originally designed to contain flow discharges of less than 1,000 m^3/s currently conveys up to 3,000 m^3/s.

The investigated section, shown in Figure 1 in the context of the entire Po basin in northern Italy, is near Boretto, 216 km from the Adriatic Sea, where the catchment area is 55,200 km^2. The alluvial bed in this section is composed of well-sorted coarse sand with a median size of $D_{50} = 0.4$ mm and a sorting of 1.2 phi. Water flows toward the southeast within an embanked, meandering channel, with a mean slope of approximately 0.15 m/km and a mean radius of curvature, R, of 1.5 km. The morphology of

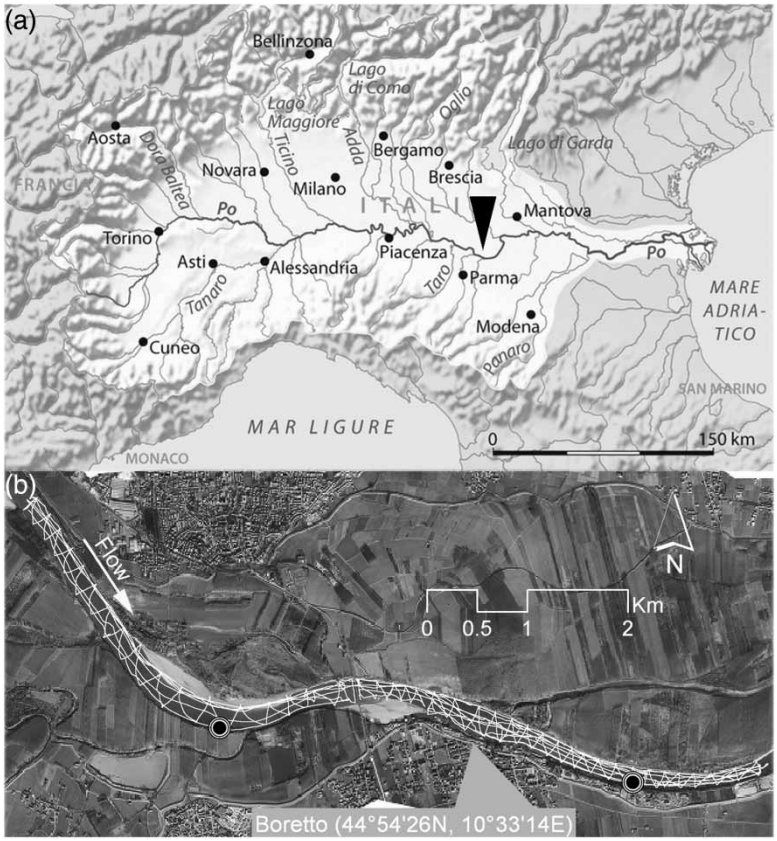

Figure 1 | The Po River Basin (a) and Po River section at Boretto ((b), corresponding to the steady-state simulations domain) with ADCP tracks from the field survey.

Downloaded from https://iwaponline.com/jh/article-pdf/15/3/813/387053/813.pdf
by guest

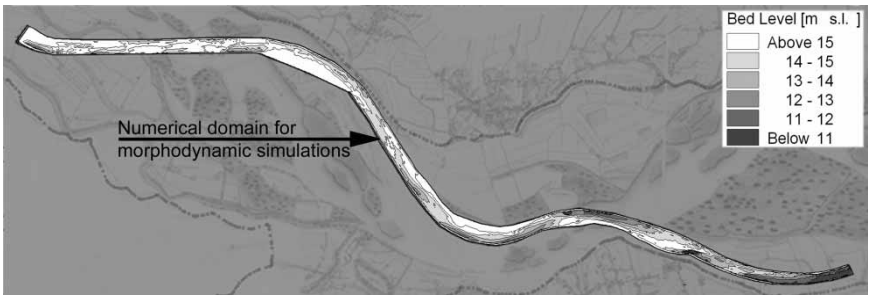

Figure 2 | Historical cartography of Po River at Boretto and 2005 bathymetry corresponding to the morphodynamic simulations domain.

the simulated section (13.5 km long and 250 m wide) is characterized by straight subsections several kilometers in length between low-curvature bends (the ratio R/B, where B is the channel width, falls within the range of 4 and 8).

A field survey was conducted on May 8, 9, and 10, 2007, at which time moderate flow conditions were present in the river after 2 dry years (May 2005–May 2007). During the field survey, the mean water level measured at the Boretto gauging station was −1.40 m, or 18.64 m above sea level (a.s.l.), with a standard deviation of 0.35 m, and the water level was lowering at a consistent rate of 0.5 m/day. The corresponding mean flow and mean flow depth were 974 m^3/s and 3.6 m, respectively. The mean depth along the thalweg was approximately 5.2 m, and the associated standard deviation was approximately 1.5 m.

The bathymetric survey was conducted using a Kongsberg EM 3000D multibeam system and gave the river channel bathymetry and bed form morphology of the 8.5-km-long section of the Po River (Figure 1) at a 1-m planimetric resolution and an RMS accuracy of 0.05 m for depth. Two Teledyne RDI ADCPs working at different frequencies (600 and 1,200 kHz) were deployed to map the depth-averaged flow field and characterize the river's suspended sediment. The ADCPs were operated on a moving vessel for the dynamic survey along the longitudinal and transverse transects (Figure 1(b)) that provided detailed maps of the: (1) magnitude of the depth-averaged velocity; (2) friction velocity; (3) angle of the near-bottom velocity with respect to the near-surface velocity; and (4) distributions of the depth-averaged concentration and suspended sediment grain size. The survey was completed in 3 days to reduce the non-stationary effects of the hydrological conditions on the surveyed data. A Trimble DSM 232 GPS Receiver was integrated with the 1,200-kHz ADCP to provide high-accuracy DGPS real-time correction data. The final position accuracy of the velocity and echo profiles was less than 0.2 m. The measured velocity difference was less than 0.05 m/s using the ADCP signal devoted to tracking the bottom or DGPS (Gordon 1996). These differences were negligible compared with the mean velocity magnitude (1 m/s). Additional details on the Po River survey can be found in Guerrero & Lamberti (2011).

MATHEMATICAL MODEL

A mathematical model of the water–sediment fluxes, bed morphology, and sediment size variation in curved alluvial rivers was applied to this case study. The model was implemented by DHI in the MIKE21C 2-D shallow water code. A detailed description of the model can be found in DHI (2002), Olesen (1987) and Talmon (1992). The analysis and verification of the mathematical model found in Olesen (1987) and Talmon (1992) is beyond the scope of this investigation, but the model's fundamental features that are relevant to the calibration in this study are reported here. In particular, the model accounts for the secondary flows, that is, the flow component perpendicular to the primary longitudinal direction, and the effect of the river bed slope on the sediment transport direction. These features make the model quasi 3-D, but introduce some parameters that require accurate calibration.

The bed level model for uniform sediment is formed by the equation of continuity for the sediment (Equation (1)), a transport rate model (Equation (2)), and a transport

Downloaded from https://iwaponline.com/jh/article-pdf/15/3/813/387053/813.pdf
by guest

direction model (Equation (3)):

$$\frac{\partial h}{\partial t} = \frac{\partial S_s}{\partial s} + \frac{\partial S_s \cdot \tan\psi}{\partial n} + \frac{S_s \cdot \tan\psi}{R} \quad (1)$$

$$S_s = S \cdot \left(1 + e \cdot \frac{\partial h}{\partial s}\right) \quad (2)$$

$$\tan\psi = \tan\delta + G \cdot \left(\frac{\theta}{\theta_0}\right)^{-a} \cdot \frac{\partial h}{\partial n} \quad (3)$$

with the following variables:

h	water depth
R	local radius of curvature of the coordinate system
t	time coordinate
s and n	longitudinal and transverse curvilinear space coordinates
S	volumetric sediment transport rate per unit width
θ	Shields parameter
θ_0	Shields parameter in the river channel axis
Ψ	angle between the sediment transport vector and s-lines
δ	bed shear stress direction angle in the s-n system
a, e and G	model parameters.

S is derived from existing formulae for sediment transport capacity assessment in uniform shear flow. These formulae give a relationship between a dimensionless transport parameter and a dimensionless bed shear stress (i.e., the Shields parameter). A review of sediment transport formulae topics can be found in Garcia (2008), among others. The mathematical models for the flow and the convection-diffusion of suspended sediment can be found in Olesen (1987) and Talmon (1992), respectively. The 2-D convective-diffusive equation adopted in the model assumes equilibrium of the sediment concentration near the bed by following Galappatti's (1983) approach for a quasi-steady concentration profile.

The bed shear stress representation in the depth-integrated flow model, or 2-D scheme, is particularly relevant to the calibration performed here. The bed shear stress (s and n components) and direction are approximated in the model by:

$$\tau_{bs} = \rho \cdot g \frac{u^2}{C^2} \quad (4)$$

$$\tau_{bn} = \rho \cdot g \frac{u}{C^2}(v + u \cdot \tan\delta_s) \quad (5)$$

$$\tan\delta = \frac{v}{u} + \tan\delta_s \quad (6)$$

with the following variables:

ρ	density of water
g	gravitational acceleration
C	Chezy parameter
u and v	depth-averaged velocity components in the s and n directions
δ_s	angle between the streamline and bed shear stress, i.e., bed shear stress angle.

The bed shear stress angle, δ_s, due to secondary flows is implemented in the model as a first-order function (Kalkwijk & Booij 1986; Olesen 1987) according to the relationship:

$$\lambda \cdot \frac{\partial(tg\delta_s)}{\partial s} + tg\delta_s = -\beta \cdot \frac{h}{R_s} \quad (7)$$

where λ is the adaptation length of the bed shear stress angle due to secondary flow, R_s is the streamline curvature radius, and the β parameter represents the dampening effect of bed friction on the forcing term (i.e., the ratio of the water depth to the curvature radius). The adaptation length, λ, is assumed to be proportional to the water depth-Chezy parameter product. Therefore, λ has a low value for a low water depth over a rough bed. The Equation (7) partial derivative is negligible in this case, and the streamline curvature immediately triggers shear stress angle near the bed. Conversely, λ has a high value for a high water depth over a smooth bed. In this case, the lag between the bed shear angle and forcing flow is not negligible. The β parameter is modeled as follows:

$$\beta = \alpha \cdot \frac{2}{k^2}\left(1 - \frac{1}{k \cdot C}\right) \quad (8)$$

Downloaded from https://iwaponline.com/jh/article-pdf/15/3/813/387053/813.pdf
by guest

where k is the von Karman constant and α is the secondary flow parameter.

The verification of the bed shear stress direction model on the basis of the mapped velocity field using ADCP recording was a major task in this study. According to Olesen (1987), the vertical distribution of flow velocity is almost symmetric with respect to the half depth and regardless of the assumed mixing length model (e.g., logarithmic, power, or von Karman velocity profile) and the C value. This symmetric distribution means that flow transverse velocity distributions close to the water surface and the river bed are fairly similar except in their signs and that a transverse zero velocity is located near the half depth. Thus, the angle between the bed flux (i.e., the sediment flux near the bed) with respect to mean flow direction (i.e., the streamline direction) was assumed equal to half the angle between the near surface and near bed fluxes of water. Furthermore, the bed flux was assumed to be parallel to the bed shear stress. The angle between the near surface and near bed fluxes was mapped from ADCP profile of water velocity and, given the described symmetric distribution, one-half was used for comparison with the simulated bed shear stress angle in Equation (7).

The balance between the secondary flow and bed slope effects on sediment transport direction (Equation (3)) changes the resulting morphology. In fact, the secondary flow diverts sediment loads from the mean flux direction, producing a lateral deposition that increases the side-slope of the channel cross-section. Such a cross-sectional shape (i.e., a transverse bed slope) triggers gravitational sliding of the sediments, counteracting lateral deposition and leveling the channel cross-section. Therefore, the model parameters in Equations (2)–(5), and (8) (including the Chezy parameter) must be carefully calibrated to reliably simulate the sediment transport direction effect on a river channel's morphology. In particular, the G, a, e, and β parameters, according to Olesen (1987), Talmon (1992) and Struiksma & Klaassen (1988), fall within the intervals 0.0–3.0, 0.5–1.0, 1–10, and 4–12, respectively, and are strongly dependent on the particulars of the case study.

The morphological model is also intended for use with non-uniform sediments (Olesen 1987). The sediment mixture is divided into a number of discrete size fractions, and a sediment transport formula and Equation (1) are applied to model the sediment continuity for each size fraction.

NUMERICAL SIMULATIONS

To perform long-term morphodynamic simulations more rapidly, the mathematical model of the water–sediment fluxes, bed morphology, and sediment size variation is solved using a quasi-steady approach within the MIKE21C code. For this reason, the code is particularly well suited to long-term and slowly varying morphodynamic simulations and is therefore usually employed to predict the impact of hydraulic works and their effectiveness in modifying a river channel's morphology.

MIKE21C was applied to the investigated section of the Po River (Figure 1(b)). Specifically, the bed roughness was first adjusted in the model by comparing the simulated to measured (1) longitudinal slopes of water free surface, and (2) and flow velocity maps. The simulated data correspond to steady-state conditions of 500, 1,000, 2,000, and 3,000 m^3/s, and of the May 2007 survey (i.e., 974 m^3/s), whereas the measured values are from the years 2005–2007 and the May 2007 survey. In these years, the longitudinal slope falls within the interval 0.11×10^{-3}–0.16×10^{-3} corresponding to flow discharge in the range 250–4,000 m^3/s. The shear stress angle δ_s was then calibrated in the model with the β and α parameters and on the basis of the velocity field maps gleaned from the 1,200 kHz ADCP survey in May 2007.

MIKE21C was also applied to the 2005 MBES bathymetry (Figure 2) derived from the extensive laser scan-bathymetric campaign carried out on the Po River in 2005 (Compagnia Generale Riprese aeree S.p.A. 2006); in this case, the morphodynamic simulations covered the 2-year period from May 2005 to May 2007. The simulations ended on the survey date in May 2007. To perform a sensitivity analysis on the simulated morphology, several values of the G and α parameters were tested, thereby modifying the balance between the effects of the secondary flow and bed slope on the sediment transport direction.

The curvilinear grid implemented here, which had a 20×12-m^2 cell on average, used the May 2007 bathymetry of the 8-km-long channel surveyed (Figure 1(b)) and the 2005 bathymetry (Figure 2) for the steady-state and morphodynamic simulations, respectively. The morphodynamic simulations were conducted on a longer stretch of the Po

Downloaded from https://iwaponline.com/jh/article-pdf/15/3/813/387053/813.pdf
by guest

River (compare Figure 1(b) to Figure 2) that incorporated an additional 6 km to move the boundary conditions further upstream.

The river bed was modeled with a single layer of sand consisting of four fractions, and the applied distribution was obtained by averaging the grain-size distributions of four samples. Figure 3 shows the sample distributions, locations, and the corresponding averaged distribution that was used in the model. The modeled bed layer was characterized with an initial homogeneous thickness equal to 4 m, which is twice the amplitude of the observed alternate bars. Furthermore, the sediment transport capacity was linearly limited in the model when the layer thickness became smaller than the fixed equilibrium thickness of 2 m (the amplitude of observed alternate bars). In this case, the sediment transport rate was multiplied by the ratio between the current and equilibrium thicknesses. The sediment transport boundary condition was attributed to the fractions represented with respect to the bed layer's current composition; that is, the boundary condition for each fraction was proportional to the percentage of that fraction in the bed layer.

Boundary conditions and preliminary analysis

The downstream condition for water level and upstream condition for discharge were inferred from the water stage measurements and the river cross-section's water stage–discharge relationship at Boretto; both data series were provided by the Po Agency. Figure 4(a) depicts the duration of the flow discharge at Boretto as calculated by the water stage–discharge relationship for the simulation period (May 2005–May 2007, square symbols) and the 45-year historical time series (1944–1989, circles).

Aiming to compare literature data and analytical assessments of sediment transport to model results, the May 2005–May 2007 and the 45-year historical periods were analyzed

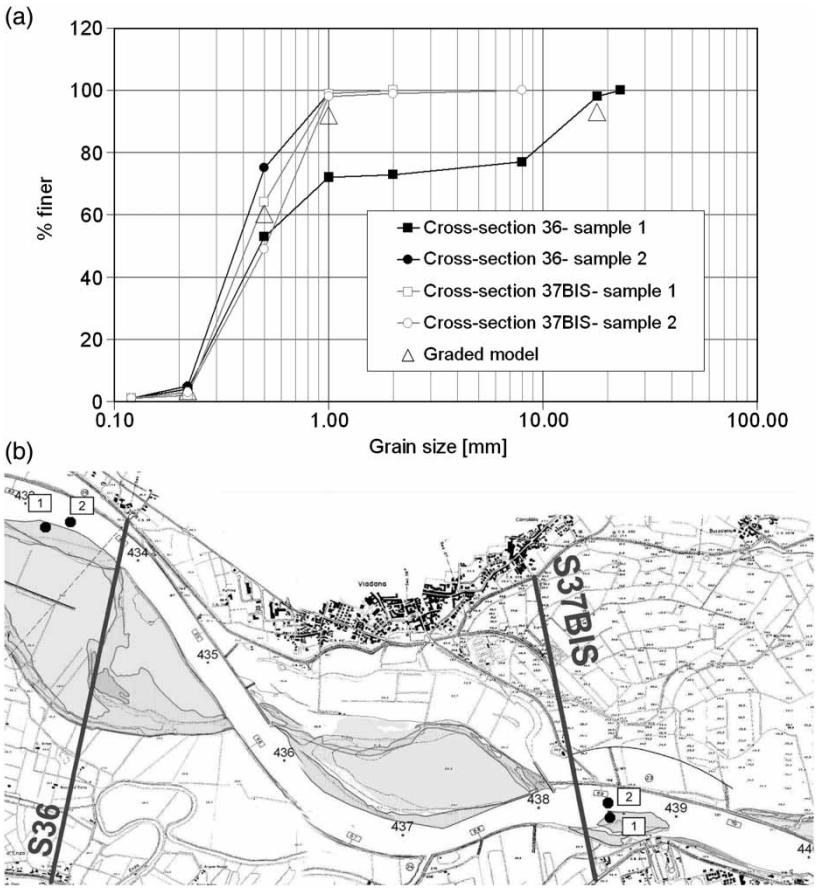

Figure 3 | Bed sediment grain-size distributions (a) and corresponding locations (b).

Downloaded from https://iwaponline.com/jh/article-pdf/15/3/813/387053/813.pdf
by guest

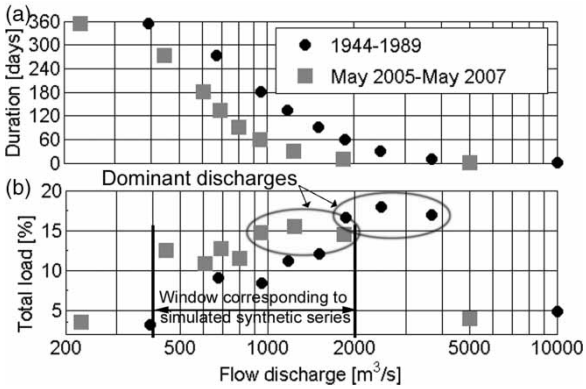

Figure 4 | Flow duration (a) and corresponding total load (b) for the simulation and historical time periods.

in terms of dominant or effective discharge, that is, the flow that cumulates most of the channel bed sediments (Biedenharn *et al.* 1999). Given the Schaffernak approach (Garde & Ranga Raju 1977), the effective discharge was assessed as the modal value of the product of stream flow frequency and sediment transport. The results in terms of the water–sediment discharge relationship are shown in Figure 4(b), in which the higher dots indicate the dominant discharge on the horizontal axis. The total load values are reported as a percentage of the cumulative sediment volume per year using the Engelund & Hansen (1967) formula at Boretto cross-section. The results show that the discharge conveying the greatest volume of sediment per year (i.e., the dominant discharge) dropped by half between the historical and simulation periods. As Table 1 shows, the cumulative volume per year in the simulation period was reduced to approximately one-third of that assessed for the 1944–1989 period, regardless of whether the Engelund & Hansen (1967) or van Rijn (1984a, b) formulae were applied.

On the basis of the performed analysis of the dominant discharge, a synthetic time series (May 2005–May 2007) of the daily flow discharge was generated to speed up the morphodynamic simulations. The synthetic series follow in the actual time series within the 400–2,000 m^3/s range, thus accounting for 80% of the cumulative volume of transported sediment per year derived from the dominant discharge analysis (Figure 4). The preliminary simulations did not indicate any appreciable deviations between the simulated morphologies using the original and synthetic time series. In fact, the synthetic time series significantly shortened the computational time by omitting data from 210 days with daily discharges of less than 300 m^3/s and 10 scattered days characterized by daily discharges of approximately 2,500 m^3/s, which eliminated 20% of the cumulative sediment volume per year. Figure 4(b) reports the flow discharge window corresponding to the synthetic time series which neglects the sediment volume under the May 2005–May 2007 distribution tails: (1) flow discharges lower than 300 m^3/s not producing an appreciable rate of sediment transport; and (2) low frequency discharges of about 2,500 m^3/s totalizing a negligible volume of sediment.

In terms of the cumulative volume of transported sediment per year, both the van Rijn and the Engelund and Hansen formulae assessments at Boretto appeared to be reliable when compared with historical data and were therefore assumed to estimate the incoming sediment discharge at the upstream fixed boundary of the model. In fact, the sediment transport per year was found to be approximately

Table 1 | Sediment transport obtained from historical data and formulae, listed in 10^6 m^3/year where not otherwise indicated

	2005–2007	1944–1989	1954–1989	20th c.
Measured turbidity (suspended and wash loads)	–	8	–	–
Estimated wash, suspended and bed loads from delta advancement	–	–	–	14
Estimated bed load from delta advancement and turbidity data at Pontelagoscuro	–	–	3	–
Engelund and Hansen assessment of suspended and bed loads	1.6	5.0	–	–
Van Rijn assessment of suspended load	1.1	3.5	–	–
Van Rijn assessment of bed load	0.5	1.5	–	–
Dominant discharge assessment using Engelund and Hansen estimation of suspended and bed loads	1,000–2,000 m^3/s	2,000–4,000 m^3/s	–	–

Downloaded from https://iwaponline.com/jh/article-pdf/15/3/813/387053/813.pdf
by guest

1.6×10^6 m^3/year in the simulation period, regardless of the formula applied. Meanwhile, the historical turbidity data, available at the Boretto gauging station for the 1944–1989 period (albeit not continuously), yielded a rate of transport of approximately 8×10^6 m^3/year, which included suspended and wash loads. The reduced dominant discharge and transport effectiveness of the 2-year period must be kept in mind when comparing the historical and analytically calculated values in Table 1.

The van Rijn formulation also provided the ratio of 30% between the bed load and total transport (neglecting wash load). Unfortunately, no measured data were available regarding bed load to compare the van Rijn assessment. Indeed, a rough estimate of the bed load was derived by considering the historical turbidity measurements available at Pontelagoscuro, the most downstream measurement station before the Po River Delta and 120 km from Boretto. The turbidity time series at Pontelagoscuro gave an estimated average suspended and wash load transport of 11×10^6 m^3/year. The total yearly sediment transport, including the previous contribution, was evaluated to be 14×10^6 m^3 on the basis of historical maps of delta advancement. The difference between these two values, equal to 3×10^6 m^3 per year, was assumed to be a rough estimate of the Po River's bed-load transport over the last century, which amounts to approximately 20% of the total (i.e., suspended and bed loads plus wash loads) in the same period.

CALIBRATION OF THE HYDRODYNAMICS MODEL

A sensitivity analysis was performed on the longitudinal average slope of the simulated water surface by testing different roughness parameters. The hydrodynamic module was also applied to simulate the hydrological steady-state condition represented by the mean flow rate and water level values at Boretto over the 3-day survey campaign, equal to 974 m^3/s and 18.64 m a.s.l., respectively.

To analyze water-slope sensitivity to bed roughness, four steady-state conditions were simulated: at 500, 1,000, 2,000, and 3,000 m^3/s. The observed period (2005–2007) covered a range of water slopes from 0.11×10^{-3} to 0.16×10^{-3}, which corresponded to discharges from 250 to 4,000 m^3/s. These values of the longitudinal slope, which were to be compared with the simulated free surface, were assessed using the difference between level measurements at the Casalmaggiore, Boretto, and Borgoforte gauge stations. The Casalmaggiore–Boretto–Borgoforte section is approximately 45 km long, with Boretto approximately in the middle, and does not contain appreciable changes to the river's flow discharge within its boundaries.

The Gauckler–Strickler parameter, k_s, was modified within the range of 33–38 m$^{1/3}$/s at the given flow discharges and downstream water levels (i.e., boundary conditions). Figure 5 shows the simulated and derived (from the difference in water levels) water slopes over the corresponding discharge.

The model did not simulate the observed scatter of the water surface slope for a given flow discharge, but the corresponding mean values were accurately simulated depending on the fixed value of k_s. Taking 36 m$^{1/3}$/s as a fixed Gauckler–Strickler parameter gave the lowest deviations between the simulated and observed water slopes over the entire discharge domain, although a positive correlation between k_s and flow discharge can be argued, which is why the best-fit line for the discharge-slope dataset is also presented in Figure 5. This fit line corresponds to the simulated water slope obtained when Equation (9) was assumed for k_s. The water depth in this equation is the mean value over the simulated section at a given flow discharge, and the assumed relationship between the Chezy and Gauckler–Strickler parameters is also reported:

$$k_s = 32.6 \cdot h^{0.05};\ C = k_s \cdot h^{\frac{1}{6}} \tag{9}$$

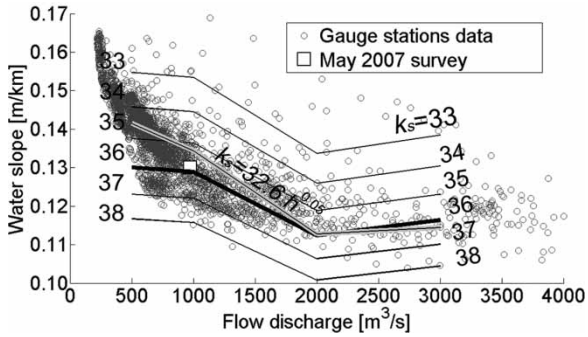

Figure 5 | Simulated discharge–water slope relationship for different Gauckler–Strickler k_s values and measured discharge–water slope pairs.

Downloaded from https://iwaponline.com/jh/article-pdf/15/3/813/387053/813.pdf
by guest

The bed roughness of the river channel was also inferred from the ADCP profiling of the water velocity during the May 2007 survey. The depth-averaged velocity, friction velocity and depth maps (Guerrero & Lamberti 2011) were used to assess the distribution of the Chezy parameter, which appeared to be weakly correlated (a correlation coefficient of less than 0.1) with the local water depth, and its resulting average value was equal to 46 $m^{1/2}/s$, corresponding to a Gauckler–Strickler parameter of 36 $m^{1/3}/s$. These field results are in good agreement with the sensitivity analysis. In fact, the measured and simulated (given k_s equal to 36 $m^{1/3}/s$) water slopes were equal to 0.13×10^{-3} for the steady-state condition of May 2007 (i.e., 974 m^3/s) and the corresponding point is very close to 36 $m^{1/3}/s$ line from the sensitivity analysis in Figure 5. The simulated distribution of the water depth for 974 m^3/s follows in the surveyed bed morphology in Figure 6 given the best value for k_s (i.e., 36 $m^{1/3}/s$).

Figure 7 depicts a comparison between the simulated and measured velocity fields, with the measured field derived from the ADCP profiling performed in May 2007 and simulation results obtained with a k_s value of 36 $m^{1/3}/s$. Inspection of Figure 7 shows that the simulated and measured 2-D velocity distributions are fairly similar throughout the entire domain. The alternate bar morphology observed in the field gives rise to a typical alternating pattern of low and high velocity values. The largest velocities in both the simulated and surveyed velocity fields developed above the bar trough, or shifted slightly downstream of the maximum depth location. This phase displacement was due to the flux vertical contraction that took place at low water depths along the stoss side of the bars. The more obvious bar protruded into the first bend, located at point 'a' in Figures 6 and 7, and the maximum velocity was located at point 'b,' which was downstream of the bend apex. Quantitative deviations are present despite the qualitative agreement of the results. The map of velocity differences in Figure 7 shows significant positive and negative deviations located at the upstream straight subsection. The extended grid (shown in Figure 2) was applied to the next morphodynamic simulations to limit the effect of the inflow distribution at the upstream boundary when producing the differences between velocity fields. Further deviations, albeit at a lower magnitude and sporadically distributed, were also observed along the entire section. These differences reflected the limits of the model when simulating sudden modifications driven by unrepresented short-scale morphology. These limits notwithstanding, the root mean square of the mapped differences (Figure 7) was approximately 10%, that is, the minimum for simulated maps with k_s values ranging from 33 to 38 $m^{1/3}/s$ and a flow discharge of 974 m^3/s.

The best agreement between the simulated and field-estimated angle of bed shear stress (δ_s in Equation (7)) was obtained by fixing the α parameter to 0.25 in Equation (8), corresponding to a β of 3 in the same equation. The measured and simulated angles are compared in Figure 8, with the measured fields derived from the ADCP profiling performed in May 2007 and simulation results with a k_s value equal to 36 $m^{1/3}/s$. Both maps show similar patterns and root mean squares of approximately 0.7°. The model captured the approximately 1–2 km wavelength of the oscillatory pattern driven by the observed alternate bars. The angle appeared to be dominated by the river curvature, especially for the flux throughout consecutive bends. Figure 8 also presents a map of the difference between the

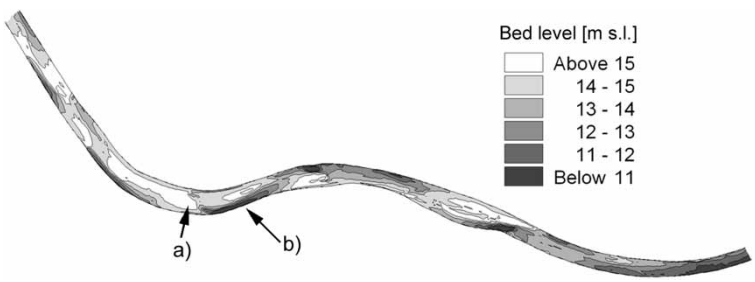

Figure 6 | Surveyed bathymetry, May 2007, corresponding to the steady-state simulations domain.

Downloaded from https://iwaponline.com/jh/article-pdf/15/3/813/387053/813.pdf
by guest

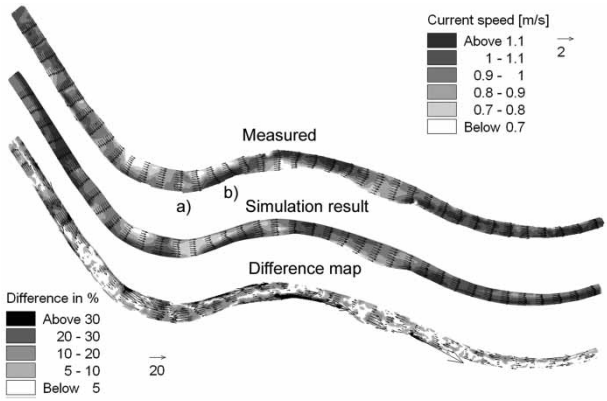

Figure 7 | Surveyed (May 2007) and simulated distributions of the depth-averaged velocity and the difference between the simulated and measured values.

simulated and measured values, indicating significant differences in the short-length scale oscillation of δ_s. Indeed, the applied model (Equation (7)) simulated longer length scale variations in δ_s that were related to: (1) the river channel curvature; and (2) the alternate bar field. Other causes (i.e., bed forms) for the shear stress angle were not taken into consideration.

CALIBRATION OF THE MORPHOLOGICAL MODEL

A sensitivity analysis of different combinations and ranges of following variables and parameters was conducted by qualitative evaluating the final morphologies from the simulations of the May 2005–May 2007 period. Starting

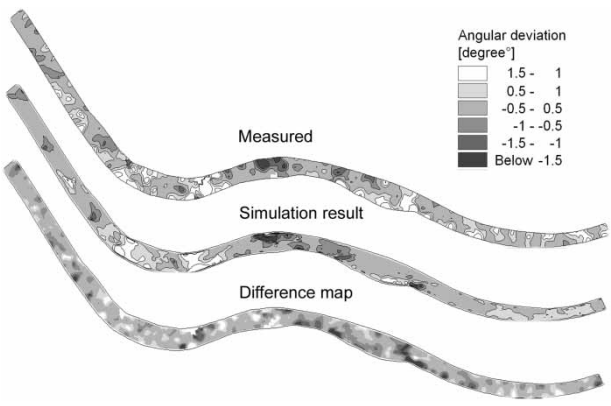

Figure 8 | Surveyed (May 2007) and simulated distributions of the near bed flux angle with respect to the depth-averaged velocity direction (counterclockwise angle is positive), and the difference between the simulated and measured values.

and final actual bathymetries are reported in Figures 2 and 6, respectively. (1) Considering the data in Table 1, the average sediment inflow (bed and suspended loads) was adjusted from 1.2×10^6 to 1.7×10^6 m^3/year in increments of 0.1×10^6 and the ratios of bed load and suspended load to total load were evaluated at 20–80% and 50–50%. (2) Given that the code simulates the bed roughness with a fixed k_s, or the Gauckler–Strickler parameter can be updated as a power law of water depth, and considering the results presented in Figure 5, either a fixed Gauckler–Strickler parameter value of 36 m$^{1/3}$/s was assumed, or Equation (9) was applied to simulate changes in bed roughness with changing hydrological conditions. (3) α (Equations (7) and (8)) oscillated within the interval 0.0–0.5. 4) G, a, and e (Equations (2) and (3)) were varied within the intervals 0.5–2.5, 0.5–1.0 and 1–5, respectively.

Approximately 50 combinations were simulated, and the most significant results are presented and discussed in this paper. The final morphologies were evaluated with respect to the actual bathymetry (Figure 6).

An average sediment inflow of 1.4×10^6 m^3/year resulted in the lowest deviation between the simulated and surveyed bathymetry (Figure 6) and was fairly close to analytical estimations listed in Table 1. The sediment transport capacity allocation between the bed and suspended loads and the bed roughness modifications within the simulated ranges only slightly affected the resulting channel morphology, while the influence of the balance between secondary flow and bed slope appeared to be relevant. Table 2 qualitatively summarizes the sensitivity of the simulated morphology to the different parameters and their corresponding values for two classes of the resulting morphologies (i.e., bend- and alternate bar-dominated).

Figure 9(a) illustrates the simulated final morphology corresponding to two of the different sets of tested parameters that gave rise to the representative morphology dominated by either bend curvature or alternate bars. Table 3 lists the parameter sets for the two representative simulations, hereafter referred to as A and B.

The variation over time for one alternate bar in simulation B is presented in Figure 10, which illustrates the time series of the bed level and mean grain size of the bed layer at the upstream bend apex (point $x3$ in Figure 9) together with the upstream boundary condition upon

Downloaded from https://iwaponline.com/jh/article-pdf/15/3/813/387053/813.pdf
by guest

Table 2 | Sensitivity of the channel morphology to calibration parameters

	Bed load (%)	Gauckler–Strickler, k_s	Secondary flow, α	Transverse slope, G, a	Longitudinal slope, e
Morphology sensitivity	Low	Very low	Fairly high	High	Very low
Resulting morphology					
Bend-dominated	Low value	High value	High value	Low values	Low values
Resulting morphology					
Alternate bar-dominated	High value	Low value	Low value	High values	High values

discharge (i.e., the synthetic time series). An increase in the bed level implied the formation of bars during low discharge periods in winter and summer, while moderate and high discharge during humid periods triggered the fast migration of bars, as reflected by the sharp decrease in bed level. Inspection of Figure 10 suggests a negative correlation between the bed level and grain size of the bed layer. The same figure also shows that the May 2007 (i.e., close to day 720) survey was performed at the end of a three-month period of moderate flow conditions, producing the observed alternate bar field (Figure 6).

Figures 11(a) and 11(b) illustrate the final distribution of depth-averaged concentrations and that of mean grain size of the bed layer for simulation B, while Figures 12(a) and 12(b) depict the distribution of depth-averaged concentrations and that of depth-averaged grain size of suspended sediments inferred from the echoes measured with ADCPs during the May 2007 survey. These field estimates represent the outcomes of the inversion method for the two frequency backscatters. The method applied the echoes measured by Teledyne RDI-ADCPs working at two frequencies (600 and 1,200 kHz) on the same water column, as described in Guerrero *et al.* (2011). Although the accurate field assessment of the concentration and grain size fields of the suspended sediments would require the backscatter calibration on the basis of field samples, the normalized values of the corrected echoes qualitatively characterized the space distributions of the concentration and grain size given their averaged values. More details on the method's capabilities and limits can be found in Guerrero *et al.* (2011, 2012).

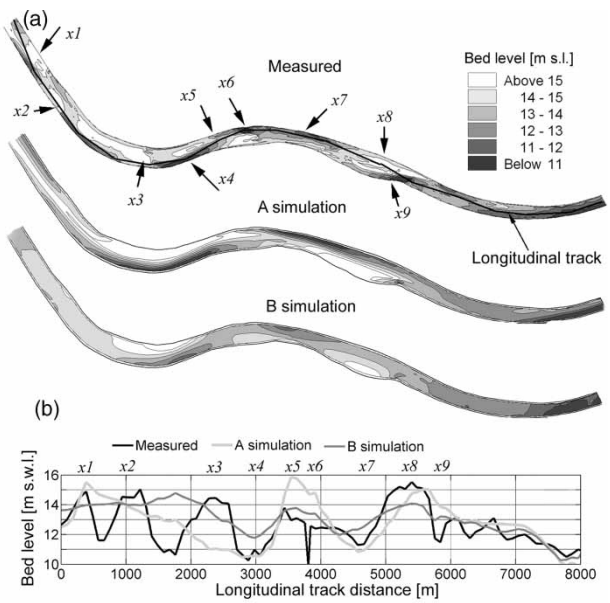

Figure 9 | Measured and simulated bathymetries (a) and comparison of measured and resulting bed levels along the longitudinal track (b).

Inspection of Figures 11 and 12 indicates a negative correlation between sediment concentration and corresponding grain size for the simulated and field data, respectively. Although the maps are characterized by variations at different length scales, the observed and modeled distributions substantiated the claim that high concentrations of fine sediment occurred at low-depth areas, corresponding to the locations where sediment deposition formed an alternate bar field during low-flow periods (Figure 10).

DISCUSSION

The calibration parameters showed a range of effectiveness at changing the river channel's morphology. No significant changes were observed in the resulting morphology when assuming a fixed Gauckler–Strickler parameter of 36 $m^{1/3}/s$ or variations with water depth, as in Equation (9). Both bed roughness models available in the code (i.e., the fixed

Downloaded from https://iwaponline.com/jh/article-pdf/15/3/813/387053/813.pdf
by guest

Table 3 | Calibration parameters for simulations A and B

Simulation name; Resulting morphology type	Total-load (10^6 m^3/year); Bed load %	Gauckler–Strickler, k_s	Secondary flow, α	Transverse slope, G, a	Longitudinal slope, e
A) Bend-dominated	1.4; 30	36	0.25	0.5, 0.5	5
B) Bar-dominated	1.4; 30	36	0.40	2.5, 0.5	5

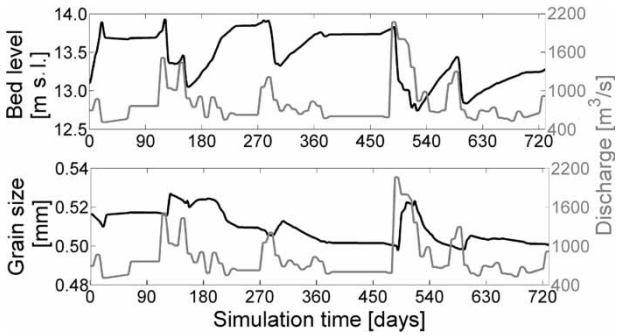

Figure 10 | Simulated bed level and grain size of the bed layer at the upstream bend apex and imposed discharge at the upstream boundary.

Gauckler–Strickler value and the water depth power law) reasonably simulated measured water slopes within the range of 1,000–3,000 m^3/s (Figure 5). This range also includes the dominant discharge interval (Figure 4(b)) for the morphodynamics simulation period (i.e., May 2005–May 2007). Deviations arose between the simulated water slopes at lower discharges with options (Figure 5), but these deviations did not significantly affect the simulated morphology because of the low discharge values.

The small observed effect of the longitudinal slope parameter e and the high impact of the secondary flow and transverse slope parameters (α, G, and a) on the resulting morphology can be understood by examining Equations (1)–(8). The bed shear stress direction, δ, and bed transverse slope had similar order of magnitudes affecting the sediment transport direction model (Equation (3)), whereas the longitudinal slope was far lower than unity and therefore negligible in the transport rate model (Equation (2)). These order of magnitudes made the sediment transport model (Equations (1)–(3)) sensitive to the α, G and a parameters, which were therefore accurately calibrated.

The allocation between the bed and suspended loads for a given total load directly affected the sediment transport continuity equation (Equation (1)) by changing the sediment transport per unit width at the bed. Therefore, a smaller bed load fraction and larger suspended load fraction decreased the final morphology's sensitivity to the bed transverse slope. A slight reduction in the local slope's effect on the resulting morphology was observed when decreasing the bed load percentage. The accurate simulation of the sediment transport direction (Equation (3)) appeared to be much more important to the resulting morphology. The secondary flow parameter α was kept equal to 0.25 in simulation A to agree with the May 2007 survey. In fact, an α value equal to 0.25 yielded the best agreement between

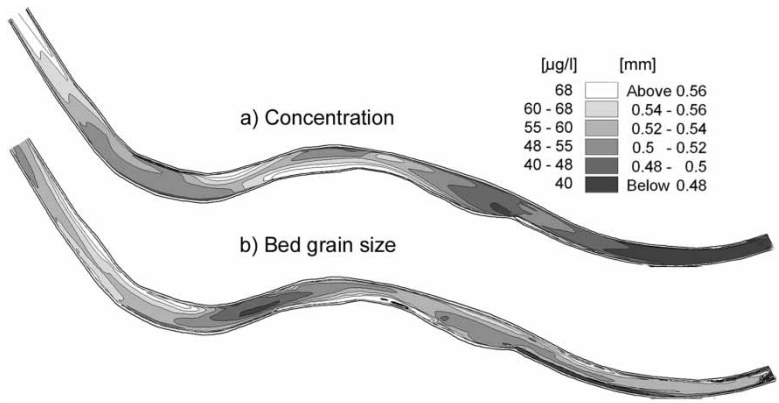

Figure 11 | Simulated distributions of the depth-averaged concentration and bed layer's mean grain size.

Downloaded from https://iwaponline.com/jh/article-pdf/15/3/813/387053/813.pdf
by guest

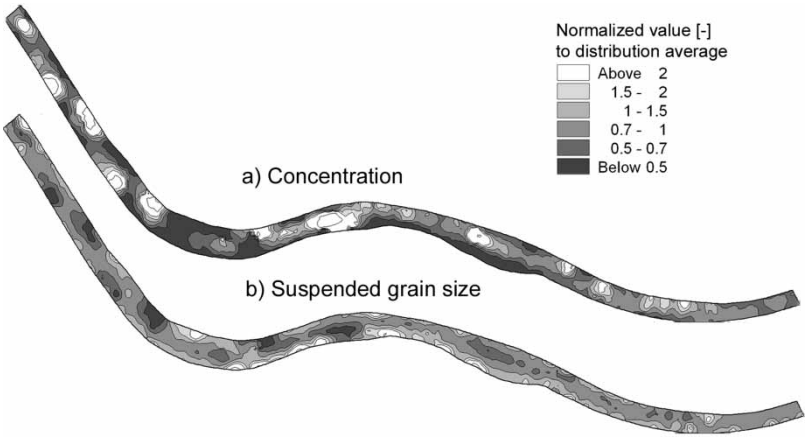

Figure 12 | Measured distributions of the depth-averaged concentration and suspended grain size.

the measured and simulated angle of the near bed flux for the May 2007 simulation. The variation in the direction of near bed flux with flow discharge could be investigated by mapping the corresponding angle at different hydrological conditions with ADCP, albeit within the sensitivity analysis performed on the final morphology, the α parameter had less of an effect than the G parameter. Two opposite limits to the G parameter were presented. A low G value of 0.5 was used in simulation A to minimize the gravitation effect that would trigger lateral deposition slides, while a higher value of 2.5 was assumed for simulation B with the goal of maximizing sediment sliding. Parameter α was then fixed at 0.4 for simulation B in an attempt to partially balance the effect of an increased G value in Equation (3). Parameter a was disregarded and therefore maintained at 0.5 for both simulations because G acted likewise in Equation (3).

The comparison of the simulated and measured morphologies (Figure 9) supported the importance of the balance between secondary flow and gravitational effect in reproducing the final morphology. Bars with shorter wavelengths, shown in Figure 9(a) in cross-sections $x1$ and $x2$, were not represented by either simulation, being in some way grouped along the entire upstream subsection (i.e., from $x1$ to $x3$). The morphology in simulation B may have been more accurate within the $x3$–$x6$ subsection, where it caught the elevation drop in cross-section $x3$ and the degree of deposition at cross-sections $x5$–$x6$. Simulation A was more accurate at representing the degree of erosion in $x4$ and was preferable for the simulation of the $x7$–$x8$ subsection. The concentrated erosions in $x6$ and $x9$ were produced from the ruins of a submerged groin and Boretto port dredging activities, respectively, and were fairly small to be represented effectively at the model scale.

The final morphologies from simulations A and B appeared to be dominated by bend curvature and alternate bars, respectively, and depended mostly on parameter G, which fixed the gravitational sliding effect in the sediment transport direction, and to a lesser degree on parameter α, which fixed the secondary flow intensity. In fact, given a G value equal to 2.5, α values ranging from 0.0 to 0.5 did not affect morphologies similar to those produced by simulation B. α values larger than 0.5 were too far from 0.25 value inferred from the calibration of near bed flux angles (Figure 8). The importance of the secondary flow parameter to the simulated morphology was more evident at lower values of G. The simulated morphology was close to that produced by simulation A in such cases, but resulted in a higher or lower degree of bed changes for α values equal to 0.5 or 0.0, respectively.

Resulting morphologies reflected the model's limits when simulating shorter length scale variations in observed bathymetry and the corresponding sediment maps (Figures 9, 11, and 12) and clearly illustrated the smoothing of variations inherent to the 2-D numerical scheme. The code reproduced only longer length scale variations over the computational domain, and the high G value in simulation B was an attempt to overcome that limit by increasing the bed transverse slope

Downloaded from https://iwaponline.com/jh/article-pdf/15/3/813/387053/813.pdf
by guest

effect on the sediment transport direction. Indeed, simulation B produced a reasonable representation of the bar dynamics over time (Figure 10) and the corresponding sediment sorting that was observed in the surveyed maps and that did not take place in simulation A. Simulation A accurately represented the observed maximal scours and depositions that were somehow leveled in simulation B.

CONCLUSIONS

The numerical code MIKE21C, created by the DHI for the simulation of shallow river (2-D) hydro-morphodynamics, was calibrated against detailed bathymetry and water–sediment flux maps obtained by using MBES and ADCPs on an 8-km-long section of the Po River in Italy. The comparison of these methods demonstrated how the mappings from novel, virtually non-intrusive measurement devices could be used for the calibration and validation of existing software.

The hydrodynamic module was first calibrated comparing steady-state simulation results to 3 years' recordings (2005–2007) of water level and flow discharge. The observed variation in water slope with flow discharge was appropriate simulated by assuming an almost constant Gauckler–Strickler parameter of 36 $m^{1/3}/s$, at least within the dominant discharge range (1,000–2,000 m^3/s) that is most effective at changing river channel morphology. A Gauckler–Strickler parameter equal to 36 $m^{1/3}/s$ also corresponded to the space-averaged value of the bed roughness map inferred from the May 2007 ADCP data with an actual discharge of 974 m^3/s. This evidence demonstrated that the mapping method for bed roughness could be effectively applied to the hydrodynamic calibration of a 2-D model, especially in cases where other data (e.g., water level measurements at gauge stations, water level–discharge relationships) were not available.

A sensitivity analysis of the applied morphodynamic model to its parameters was performed by simulating the 2 years prior to the survey date (May 2007). In particular, the sediment transport direction model was found to effectively affect the simulated morphology at a given bed roughness and sediment load income. The secondary flow and gravitational sliding parameters governed the sediment flux direction and were crucial in reproducing the bathymetry observed at the end of the period. The secondary flow parameter, α, was fixed at 0.25 based on the May 2007 map of the near bed flux angle with respect to mean flow direction. This method illustrated how the mappings from ADCPs could be used to fix the effect of secondary flow on the sediment transport direction.

The resulting morphologies appeared to be dominated either by bend curvature or alternate bars, and depended mostly on the assumed bed transverse slope parameter, G, to simulate the gravitational sliding effect. Direct field evidence on gravitational sliding effects was lacking, so the bed transverse slope parameter was calibrated to reproduce the observed sediment sorting at alternate bars during low flow discharge periods (e.g., in May 2007). This method demonstrated how the extensive measurement of backscattered echoes at two frequencies, which provided the concentrations and grain size maps of suspended sediments, could be used to reduce uncertainty when calibrating the sediment transport direction model. A G value of 2.5 reproduced the observed negative correlations between concentration and sediment grain size and water depth, but it also leveled the observed maximal scours and depositions that were better reproduced using a G value of 0.5.

In conclusion, the numerical code in this study was capable of reproducing longer length scale variations over the computational domain, but filtered out variations in the observed velocity-sediment field and morphology at smaller length scales.

ACKNOWLEDGEMENTS

The authors are grateful to the 'Agenzia Interregionale per il fiume Po' and the 'Autorità di bacino del fiume Po' for providing data on the Po River.

REFERENCES

Biedenharn, D. S., Thorne, C. R., Soar, P. J., Hey, R. D. & Watson, Ch. C. 1999 *A Practical Guide to Effective Discharge Calculation (Appendix A)*. U.S. Army Corps of Eng., Vicksburg, Mississippi, USA.

Cati, L. 1981 Idrografia e Idrologia del Po. Report of the Ufficio Idrografico del Po, Parma, Italy.

Downloaded from https://iwaponline.com/jh/article-pdf/15/3/813/387053/813.pdf
by guest

Compagnia Generale Riprese aeree S.p.A. 2006 Esecuzione di rilievi 'Laser-scan' del Fiume Po da confluenza Ticino all'incile, comune di Ariano nel Polesine. Report of the Autorità di bacino del Fiume Po, Parma, Italy.

DHI Water & Environment 2002 *Mike21C River Hydrodynamics and Morphology User Guide*. DHI, Horsholm, Denmark.

Engelund, F. & Hansen, E. 1967 *A Monograph on Sediment Transport in Alluvial Stream*. Teknisk Forlag, Danish Technological University, Copenhagen, Denmark.

Galappatti, R. 1983 A depth-integrated model for suspended transport. *Commun. Hydraul.* **83** (7), Dept. of Civil Engineering, Delft Univ. of Technology, The Netherlands, pp. 1–114.

Garcia, M. 2008 Sedimentation Engineering: Processes Measurement, Modelling and Practice. ASCE Manuals and Report No. 110, ASCE Publications, Reston, Virginia, USA.

Garde, R. J. & Ranga Raju, K. G. 1977 *Mechanism of Sediment Transportation and Alluvial Stream Problems*. Wiley Eastern Ltd., New Delhi, India.

Gordon, R. L. 1996 *Acoustic Doppler Current Profiler. Principles of Operation: A Practical Primer*. R. D. Instruments, San Diego, California.

Guerrero, M. & Lamberti, A. 2006 Loose-bed models for river structure design: two example studies on river Po. *Proceedings of River Flow 2006*, Lisbona, 6–8 September, 2, 1915–1922.

Guerrero, M. & Lamberti, A. 2011 Flow field and morphology mapping using ADCP and multibeam techniques: survey in the Po River. *J. Hydraul. Eng.* **137** (12), 1576–1587.

Guerrero, M., Ruther, N. & Szupiany, R. 2012 Laboratory validation of ADCP techniques for suspended sediments investigation. *Flow Meas. Instrum.* **23** (2012), 40–48.

Guerrero, M., Szupiany, R. & Amsler, M. 2011 Comparison of acoustic backscattering techniques for suspended sediments investigation. *Flow Meas. Instrum.* **22** (2011), 392–401.

Jansen, P. H., van Bendegom, L., van den Berg, J., de Vries, M. & Zanen, A. 1979 *Principles of River Engineering*. Pitman Publishing, London.

Kalkwijk, J. P. T. & Booij, R. 1986 Adaptation of secondary flow in nearly-horizontal flow. *J. Hydraul. Res.* **24** (1), 19–37.

Lamberti, A. & Schippa, L. 1994 Studio dell'abbassamento del fiume Po: previsioni trentennali di abbassamento a Cremona. Supplemento a Navigazione Interna, rassegna trimestrale di studi e informazioni, n ¾ Luglio-Dicembre 1994, Azienda Regionale per i porti di Cremona e Mantova, Cremona, Italy.

Mosselman, E. 1992 Mathematical modelling of morphological processes in rivers with erodible cohesive banks. *Commun. Hydraul. Geotech. Eng.* **92** (3), Delft University of Technology, pp. 1–133.

Olesen, K. W. 1987 Bed topography in shallow river bends. *Commun. Hydraul.* **87** (1), Dept. of Civil Engineering, Delft Univ. of Technology, The Netherlands, pp. 1–265.

Olsen, N. R. 1999 *Computational Fluid Dynamics in Hydraulic and Sedimentation Engineering*. Dept. of Hydraulic and Environmental Engineering, The Norwegian University of Science and Technology, Trondheim.

Parker, G. 2004 1D sediment transport morphodynamics with application to rivers and turbidity currents e-book. Available from: http://vtchl.uiuc.edu/people/parkerg/.

Parsons, D. R., Best, J. L., Orfeo, O., Hardy, R. J., Kostaschuk, R. & Lane, S. N. 2005 Morphology and flow fields of three-dimensional dunes, Rio Paranà, Argentina: results from simultaneous multibeam echo sounding and acoustic Doppler current profiling. *J. Geophys. Res.* **110**, F04S03.

Rennie, C. D. & Church, M. 2010 Mapping spatial distributions and uncertainty of water and sediment flux in a in large gravel bed river reach using an acoustic Doppler current profiler. *J. Geophys. Res.* **115**, F03035.

Struiksma, N. & Klaassen, G. J. 1988 Threshold between meandering and braiding. In: *Proc. International Conference on River Regime*, Hydraulics Research Limited, Wallingford, Oxon, UK, pp. 107–120.

Szupiany, R. N., Amsler, M. L., Best, J. L. & Parsons, D. R. 2007 Comparison of fixed and moving vessel flow measurements with an aDp in a large river. *J. Hydraul. Eng.* **133** (12), 1299–1309.

Szupiany, R. N., Amsler, M. L., Parsons, D. R. & Best, J. L. 2009 Morphology, flow structure, and suspended bed sediment transport at two large braid-bar confluences. *Water Resour. Res.* **45**, W05415.

Talmon, A. M. 1992 Bed Topography of River Bends with Suspended Sediment Transport. Ph.D. Thesis, Delft Univ. of Technology, The Netherlands.

van Rijn, L. C. 1984a Part I: Bed load transport. *J. Hydraul. Eng.* **110** (10), 1431–1456.

van Rijn, L. C. 1984b Part II: Suspended load transport. *J. Hydraul. Eng.* **110** (11), 1613–1641.

Viscardi, J. M., Pujol, A., Weitbrecht, V., Jirka, G. H. & Olsen, N. R. 2006 Numerical simulation on the Paranà de las Palmas River. *Proceedings of River Flow 2006*, Lisbona, 6–8 September, 1, 367–377.

Yalin, M. S. & da Silva, A. M. F. 2001 *Fluvial Processes*. IAHR Monograph, A.A. Balkema, Delft, The Netherlands.

First received 7 February 2012; accepted in revised form 12 November 2012. Available online 13 December 2012

Downloaded from https://iwaponline.com/jh/article-pdf/15/3/813/387053/813.pdf
by guest